PHILOSOPHICAL TRANSACTIONS A

royalsocietypublishing.org/journal/rsta

Review

Cite this article: Fung L, Caldag HO, Bees M. 2025 Foundation and challenges in modelling dilute active suspensions. *Phil. Trans. R. Soc. A* **383**: 20240251.
https://doi.org/10.1098/rsta.2024.0251

Received: 26 September 2024
Accepted: 14 April 2025

One contribution of 17 to a theme issue 'Biological fluid dynamics: emerging directions'.

Subject Areas:
statistical physics, fluid mechanics, biophysics

Keywords:
continuum model, biologically active suspensions, active Brownian particles, microswimmers

Author for correspondence:
Lloyd Fung
e-mails: lloyd.fung@imperial.ac.uk; lsf27@cam.ac.uk

Foundation and challenges in modelling dilute active suspensions

Lloyd Fung[1,2], Hakan Osman Caldag[3] and Martin Bees[3]

[1]Department of Applied Mathematics and Theoretical Physics, University of Cambridge, Cambridge, UK
[2]Department of Aeronautics, Imperial College London, London, UK
[3]Department of Mathematics, University of York, York, UK

LF, 0000-0002-1775-5093; HOC, 0000-0002-4394-6045

Active suspensions, which consist of suspended self-propelling particles such as swimming microorganisms, often exhibit non-trivial transport properties. Continuum models are frequently employed to elucidate phenomena in active suspensions, such as shear trapping of bacteria, bacterial turbulence and bioconvection patterns in suspensions of algae. Yet, these models are often empirically derived and may not always agree with the individual-based description of active particles. Here we review the essential coarse-graining steps to develop commonly used continuum models from their respective microscopic dynamics. All the assumptions needed to reach popular continuum models from a multi-particle Fokker–Planck equation, which governs the probability of the full configuration space, are explicitly presented. In the dilute limit, this approach leads to the mean-field model (a.k.a. Doi–Saintillan–Shelley model), which can be further reduced to a continuum equation for particle density. Moreover, we review the limitations and highlight the challenges related to continuum descriptions, including significant issues in implementing physical boundary conditions and the possible emergence of singular solutions.

This article is part of the theme issue 'Biological fluid dynamics: emerging directions'.

THE ROYAL SOCIETY PUBLISHING

1. Introduction

Active suspensions are suspensions of self-propelling (or motile) particles whose propelling direction depends on the particles' (stochastic) orientation and their biases to move towards or away from certain external stimuli (called taxes). Typical examples include suspensions of motile microorganisms, such as bacteria, spermatozoa and algae, and artificial microswimmers such as Janus particles. In soft matter and statistical physics, active suspensions are distinctive in how they are driven out of equilibrium locally when particles expend energy to maintain locomotion. From a fluid dynamics perspective, they have unusual transport properties due to the particles' motility, and their rich and complex phenomenology in flows with vanishing Reynolds number is non-trivial. The stress they exert on the flow can also give rise to peculiar rheological properties like superfluidity, which are not observed in passive fluid systems. Understanding the fundamental processes in these complex systems may benefit applications, such as the management of biofilms on surfaces, mixing and unmixing at the microscale, the modelling of phytoplankton and thus the carbon cycle in the ocean, food and beverage production and the biochemical manufacturing of medicines and biofuels [1–3].

A key challenge in modelling active suspensions is to derive a macroscopic continuum model that is tractable for analysis and interpretation, while remaining grounded in the essential physics of the microscopic dynamics. Early models [4,5] incorporated the effects of taxes by modifying the effective drift in the particle density equation. These phenomenological models could only capture certain collective behaviours qualitatively, as they did not take into account the microscopic orientational dynamics. The seminal work by Pedley & Kessler [6,7] made a significant advancement in explicitly accounting for the orientational dynamics within their continuum description. Taking inspiration from how the mean-field stresses from passive particles are modelled [8,9], they wrote down the mean disturbance due to particle motility. As for the particle transport, they used statistical moments of their orientation distribution to derive the effective drift and diffusivity due to biased motility. Although the model was based on the microscopic dynamics, the particle's effective diffusivity D remains *ad hoc* and fails to capture the theoretical $D \sim (V^c)^2/d_r$ scaling [10], as Pedley & Kessler [6] separated the orientational and spatial distribution without full consideration of the coupling between the particle's random rotation with rotational diffusivity d_r and its swimming speed V^c.

The more rigorous approach is to model the probability of the particle configuration in both position and orientation space, governed by the Fokker–Planck equation, which is derived from the microscopic Langevin equation. Hill & Bees [11] and Manela & Frankel [12] first demonstrated how the coupling between position and orientation space in the Fokker–Planck equation gives rise to an effective dispersion of active particles using the generalized Taylor dispersion (GTD) theory [13]. Later work by Saintillan & Shelley [14] wrote down the same equation and the mean-field flow equation from a kinetic theory perspective. They then used a linear stability analysis to show how the coupling between the particle configuration and the mean flow caused by particle stresses can lead to collective behaviour at a length scale much larger than the particles themselves. Subramanian & Koch [15] also independently arrived at a similar set of equations for motile bacteria, with an additional term for the run-and-tumble dynamics. Despite the apparent success of the mean-field model, its prediction of the onset of bacterial turbulence was later challenged by the supposedly equivalent simulation [16], where no discrete transition as predicted by the mean-field theory was observed. Instead, even at particle density well below the onset, they observed strong spatio-temporal correlations in the velocity fluctuations that are reminiscent of the observed turbulence. Later work by Škultéty *et al.* [17] showed that this fluctuation correlation can be captured by a careful reconsideration of the kinetic theory, where, in addition to the mean field, they have also considered explicitly the fluctuations in addition to the mean field when reducing the multi-particle description of the suspension. Their work illustrated how the implicit assumptions of a certain model might result in unforeseen yet significant repercussions. Such repercussions may not be easily evident until the model's assumptions are thoroughly scrutinized.

royalsocietypublishing.org/journal/rsta Phil. Trans. R. Soc. A 383: 20240251

Hence, the purpose of this article is to offer a thorough examination of the foundation underlying current continuum models for active suspensions, laying bare all the assumptions necessary to scale up the microscopic dynamics of individual particles to a suspension. Particular focus will be on the derivation of the mean-field model, sometimes known as the Doi–Saintillan–Shelley (DSS) model, and its limitations due to the dilute assumption. This work is not the first to present a detailed derivation towards a macroscopic model from the underlying microscopic dynamics of individual particles (see [17–19]). Here, we aim to provide a brief and precise derivation, coupled with a critical review of constraining assumptions and outstanding challenges, to aid the reader in understanding the accuracy and limitations of the model. Other practical issues, such as the high dimensionality of the model and boundary conditions, will also be discussed. Finally, we will explore the possibility of adopting coarse-graining methodologies from neighbouring fields to extend continuum modelling to concentrated suspensions.

Besides rigorous coarse-graining from the bottom up, we should also briefly mention phenomenological approaches to modelling systems of active particles. Originally developed for flocking, the Toner–Tu theory [20] proposed that a phenomenological equation can be written down by including all terms allowed by symmetry. The theory was extended to suspensions of self-propelled particles [21] and for modelling active turbulence in dense bacterial suspensions [22,23]. Another popular approach for modelling active nematic systems, such as a microtubule–kinesin mixture, is to modify the continuum equations from liquid crystal theory by including new terms arising from the activity [24]. These models are often associated with very dense systems of active particles, which are beyond the scope of this work. The review by [25] provides an overview of these phenomenological approaches and their comparisons with coarse-grained models [14,26]. Instead, here we shall focus on coarse-graining dilute suspensions of self-propelled particles where hydrodynamic interactions dominate.

The article is structured as follows. First, we quantify the trajectory and hydrodynamic disturbances arising from a single stochastic self-propelling particle in §2. Then, in §3, we consider N suspended particles and write down the equivalent N-particle Fokker–Planck equation and explain the approximation required to reduce it to the mean-field (DSS) model (§3b). The resulting one-particle Fokker–Planck equation in the DSS model can be further reduced to a particle density equation (§3c). After that, we will discuss several issues resulting from the approximations used to derive the DSS model (§4). These issues include the emergence of singular solutions due to the lack of volume exclusion in the model (§4a), difficulties in closing the many-body problem (§4b) and choice of boundary conditions (§4c). Finally, in §5, we lay out the direction and priorities in the development of continuum models for active suspensions.

2. Microscopics: Stokes flow around an active particle

We start by considering a single rigid active particle suspended in a Newtonian fluid. Given the density $\rho_f \sim 1000$ kg m^{-3} and viscosity $\mu \sim 0.001$Pa s of the fluid, the size of the particle $a \sim 10$–100 μm and the slip velocity (approx. 10–100 μms^{-1}), the particle Reynolds number $Re_p \approx 10^{-4} - 10^{-2} \ll 1$ is vanishingly small [27, figure 2.2]. Assuming that the particle j is of volume v_j and mass $v_j\rho_p$, its inertia can be neglected, as biologically active particles usually have density ρ_p close to that of the fluid ρ_f. Hence, the flow around the particle can be treated as steady and Stokesian, governed by

$$\mathbf{0} = -\boldsymbol{\nabla}_x q(\mathbf{x}) + \mu\nabla_x^2\mathbf{u}(\mathbf{x}) + \mathbf{f}, \quad \text{and} \quad \boldsymbol{\nabla}_x \cdot \mathbf{u}(\mathbf{x}) = 0, \tag{2.1}$$

where $\mathbf{u}(\mathbf{x})$ is the flow velocity at location $\mathbf{x}$, q the pressure and $\mathbf{f}$ the external forces on the fluid. Note that the flow around the particle only truly satisfies the Stokes equation below the inertial length scale $\ell_i \sim aRe_p^{-1}$. The macroscopic flow, however, can be inertial at the phenomenological scale.

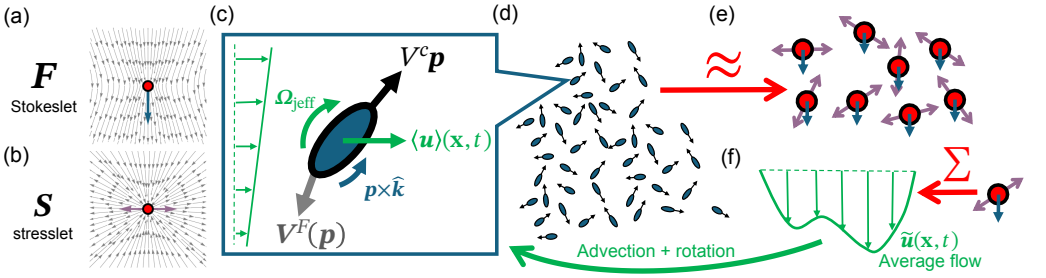

Figure 1. Particles (or swimmers) in a typical active suspension. (a,b) Disturbance flow from (a) a point force $\mathbf{F}_j$ and (b) an axisymmetric force dipole S_j. (c) Detailed view of how the locally linear flow advects and rotates a particle. (d–f) Modelling of a suspension of hydrodynamically interacting particles, in which (e) the particles are modelled as point forces and force dipoles, (f) exerting an averaged driving force on the averaged flow that, in turn, rotates and advects the particles.

(a) Disturbance flow due to an active particle

First, we consider the disturbance flow around a single particle in an otherwise quiescent flow. For zero Re_p, one can exploit the linearity of (2.1) to represent how a particle centred at $\mathbf{x}_j$ exerts stresses from its surface onto the fluid and creates a disturbance flow velocity $\mathbf{u}^d$. At a location $\mathbf{x}$ far from $\mathbf{x}_j$ (i.e. at $\mathbf{r} = \mathbf{x} - \mathbf{x}_j$, $r = |\mathbf{r}| \gg a$), this disturbance flow $\mathbf{u}^d$ can be approximated by the multipole expansions of the Green's function $\mathcal{G}$, such that

$$\mathbf{u}^d(\mathbf{r}) = (8\pi\mu)^{-1}\left(\mathcal{G}(\mathbf{r})\cdot\mathbf{F}_j + [\nabla_x \mathcal{G}(\mathbf{r})] : \mathsf{M}_j + \mathcal{O}\left(r^{-3}\right)\right), \quad \text{where} \quad \mathcal{G}(\mathbf{r}) = r^{-1} + r^{-3}\mathbf{rr}. \tag{2.2}$$

Here, $\mathbf{F}_j$ is the net force and M_j the net first moment of traction that particle j exerts on the fluid. (Note that the double contraction : is with respect to the gradient and second index of $\mathcal{G}$, i.e. $\partial_{x_c}\mathcal{G}_{ab}M_{bc}$.) Expansion up to the first-order terms is usually sufficient to represent the flow at large r, as terms at order n decay as $1/r^{n+1}$ as $r \to \infty$; a particle can be approximately represented by a point force and a point dipole in a Stokesian flow. A point force is called a Stokeslet (figure 1a) and is non-zero only when the particle experiences an external net force (e.g. buoyancy force $\mathbf{F}_j = v_j \Delta\rho_j \mathbf{g}$ due to gravity $\mathbf{g}$, where $\Delta\rho_j = (\rho_{p,j} - \rho_f)$ is the density mismatch between the particle and the fluid). The moment M_j has an antisymmetric part called a rotlet (L_j, antisymmetric force dipole) and a symmetric part called a stresslet (S_j, symmetric force dipole). These components correspond to the net torque and symmetric first moment of stresses the particle exerts on the flow, respectively. A net torque $\mathbf{L}_j$ can arise when the centre of hydrodynamic forcing is offset from the centre of the external force by a finite length ℓ_j (e.g. $\mathbf{L}_j = L_j \mathbf{g} \times \mathbf{p}$, $L_j = \ell_j v_j \Delta\rho_j$ when the particle is bottom-heavy under gravity). A stresslet S_j can arise from the particle's self-propulsion or friction against the background flow due to its inability to deform. In the absence of strong external flow, the stress generated by the self-propulsion of an active particle usually dominates over other flow-dependent dipoles, and the resulting time-averaged disturbance flow is well approximated by an axisymmetric force dipole $\mathsf{S}_j = \sigma_j \mathbf{p}_j \mathbf{p}_j$ (figure 1b) [28,29], where $\mathbf{p}_j$ is the normalized vector representing the particle's orientation. A self-propelling particle with $\sigma_j > 0$ is called a puller and $\sigma_j < 0$ a pusher.

(b) Typical trajectories of hydrodynamically interacting active particles

Now, consider N inertia-free active particles that are far apart from each other in a dilute suspension, i.e. the volume fraction ϕ is negligibly small. The configuration $\boldsymbol{\xi}_i = (\mathbf{x}_i, \mathbf{p}_i)$ of each particle i is defined by its position $\mathbf{x}_i$ and orientation $\mathbf{p}_i$. Collectively, they define the configuration of the suspension $\Xi = (\boldsymbol{\xi}_1, \boldsymbol{\xi}_2, ..., \boldsymbol{\xi}_N)$. Assuming each particle i is axisymmetric along its swimming direction $\mathbf{p}_i$, balancing the external and hydrodynamic forces from self-propulsion gives the particle's

overdamped trajectory as (c.f. figure 1c)

$$\dot{\mathbf{x}}(\mathbf{x}_i, \mathbf{p}_i; \Xi) = \mathbf{u}(\mathbf{x}_i, t; \Xi \backslash \boldsymbol{\xi}_i) + V_i^c \mathbf{p}_i + \mathbf{V}_i^F(\mathbf{p}_i). \tag{2.3}$$

Here, $V_i^c \mathbf{p}_i$ represents the self-propulsion, $\mathbf{V}_i^F(\mathbf{p}_i)$ represents the orientation-dependent translational velocity due to external force $\mathbf{F}_i$ and $\mathbf{u}(\mathbf{x}_i, t; \Xi \backslash \boldsymbol{\xi}_i)$ represents the passive advection by the flow at time t, which includes both the background flow and the disturbance from $\Xi \backslash \boldsymbol{\xi}_i$, which is the ensemble of particles other than itself. In other words, the trajectory of a particle i depends on the configuration of all other particles in the suspension. We further assume that particles are sufficiently small relative to the flow length scale such that Faxén corrections can be omitted (cf. §4a).

Similarly, the inertia-less torque balance provides the rotational dynamics as (cf. figure 1c)

$$\dot{\mathbf{p}}\left(\mathbf{x}_i, \mathbf{p}_i; \Xi\right) = \left(\boldsymbol{\Omega}_{\text{jeff}}\left(\mathbf{u}\left(\mathbf{x}_i, t; \Xi \backslash \boldsymbol{\xi}_i\right), \mathbf{p}_i\right) + \beta_i \mathbf{p}_i \times \hat{\mathbf{k}}_i\right) \times \mathbf{p}_i, \tag{2.4}$$

$$\boldsymbol{\Omega}_{\text{jeff}}\left(\mathbf{u}, \mathbf{p}_i\right) = \frac{1}{2}\boldsymbol{\Omega} + \alpha_i \mathbf{p}_i \times \mathtt{E} \cdot \mathbf{p}_i, \tag{2.5}$$

where $\boldsymbol{\Omega}_{\text{jeff}}$ is the rotation due to $\boldsymbol{\Omega} = \boldsymbol{\nabla}_x \times \mathbf{u}$ the vorticity and $\mathtt{E} = (\boldsymbol{\nabla}_x \mathbf{u} + \boldsymbol{\nabla}_x \mathbf{u}^T)/2$ the rate-of-strain of the local flow, governed by the Jeffery's equation (2.5) [30], which applies to any axisymmetric particle, in which α_i depends on the particle's shape and has the value $\left(\text{AR}_i^2 - 1\right) / \left(\text{AR}_i^2 + 1\right)$ for a spheroidal particle with aspect ratio AR_i. Meanwhile, the last term of (2.4) models any restoring torque arising from bottom heaviness [7] or preferred sedimentation orientation [31], in which β_i quantifies the timescale of the restoration and the unit vector $\hat{\mathbf{k}}_i$ points towards the preferred orientation, which is usually in the opposite direction to $\mathbf{F}_i$. As for asymmetric or shape-changing particles, readers can refer to a recent review by Ishimoto [32] on the impact of particle asymmetry on their generalized Jeffery orbits.

Most active particles are large enough that Brownian diffusion due to thermal fluctuation is insignificant. However, imperfections or variations in actuation that induce self-propulsion can incur an effective stochasticity to their trajectories. For simplicity, here we model an active suspension as a system of N active Brownian particles, each of which has a trajectory i given by

$$d\mathbf{x}_i(\mathbf{x}_i, \mathbf{p}_i; \Xi) = \dot{\mathbf{x}}(\mathbf{x}_i, \mathbf{p}_i; \Xi)dt + \sqrt{2D_T}d\mathbf{W}_x; \tag{2.6}$$

$$d\mathbf{p}_i(\mathbf{x}_i, \mathbf{p}_i; \Xi) = \dot{\mathbf{p}}(\mathbf{x}_i, \mathbf{p}_i; \Xi)dt - 2d_r\mathbf{p}_i + \sqrt{2d_r}d\mathbf{W}_p \times \mathbf{p}_i. \tag{2.7}$$

Here, D_T and d_r are the translational and rotational diffusivities that model the biological stochasticity, respectively, and $\mathbf{W}_x$ and $\mathbf{W}_p$ are the Wiener processes in translation and rotation, respectively. Both processes are assumed to have zero mean and unit isotropic variance. Note that (2.7) is interpreted in the Ito sense, and thus the rotation requires an extra $-2d_r\mathbf{p}_i$ term to conserve the unity norm. Due to the orientation-dependent propulsion or translation, the dispersion effect with rotational noise [11,12] is usually more significant than the diffusion due to translational noise (see §3c). However, the translation noise can also be significant when the particle is in very close proximity to boundaries (see §4c).

While ((2.3)–(2.7)) form a complete description of the trajectories of particles i in a given flow field, the flow field also depends on the configuration of other particles. More specifically, the flow $\mathbf{u}$ at a certain location $\mathbf{x}$ is disturbed by the forcing $\mathbf{F}_j$ and $\mathtt{M}_j$, which are from other particles, and is governed by the incompressibility condition $\boldsymbol{\nabla}_x \cdot \mathbf{u} = 0$ and the Navier–Stokes equation

$$\rho_f(\partial_t \mathbf{u} + \mathbf{u} \cdot \boldsymbol{\nabla}_x \mathbf{u}) = -\boldsymbol{\nabla}_x q + \mu \nabla_x^2 \mathbf{u} + \textstyle\sum_j (\mathbf{F}_j + \mathtt{M}_j \cdot \boldsymbol{\nabla}_x)\delta(\mathbf{x} - \mathbf{x}_j) - \frac{1}{V}\sum_j \mathbf{F}_j. \tag{2.8}$$

For the flow external to the particles, $\mathbf{u} = \mathbf{u}(\mathbf{x}, t; \Xi)$, the summations in (2.8) are for $j = 1, 2, ..., N$, whereas the flow experienced by the i-th particle $\mathbf{u}(\mathbf{x}_i, t; \Xi \backslash \boldsymbol{\xi}_i)$ will exclude the force on the particle itself ($j = 1, 2, ..., i-1, i+1, ..., N$). Note that the sum of external forces averaged over the

domain volume V is subtracted to conserve momentum in the fluid.[1] The full Navier–Stokes equation is invoked here as the macroscopic bulk flow can still be nonlinear and unsteady despite the Stokesian microscopic flow around each particle. Indeed, in some phenomena, such as bioconvection, the nonlinear and unsteady terms play a significant role at the phenomenological scale [7,34]. However, coarse-graining the stochastic and nonlinear partial differential equation (PDE) (2.8) is very difficult. Therefore, in the following derivation, we shall assume that we have effectively a Stokesian bulk flow. Linearity and the vanishing ϕ approximation allow the superposition $\mathbf{u}(\mathbf{x}_i, t; \Xi \backslash \boldsymbol{\xi}_i) = \sum_{j=1, i\neq j}^{N} \mathbf{u}_j(\mathbf{x}_i; \boldsymbol{\xi}_j(t))$, where $\mathbf{u}_j$ is the flow due to the presence of each particle j, governed by (2.1) with $\mathbf{f}$ substituted by $(\mathbf{F}_j + \mathtt{M}_j \cdot \boldsymbol{\nabla}_x)\delta(\mathbf{x} - \mathbf{x}_j) - \mathbf{F}_j/V$. Equations (2.3)–(2.7) and solution to $\mathbf{u}$ form a complete description of the active suspension, but a direct integration is difficult and likely analytically intractable. Therefore, coarse-graining is necessary.

3. Coarse-graining through reducing the Fokker–Planck equation

For the set of stochastic equations (2.6) and (2.7) for N particles, one can write down the equivalent N-particle Fokker–Planck equation,

$$\partial_t \Psi_N(\Xi, t) = \sum_{i=1}^{N} \left\{ \boldsymbol{\nabla}_{x_i} \cdot \left[-\dot{\mathbf{x}}(\mathbf{x}_i, \mathbf{p}_i; \Xi)\Psi_N + D_T \boldsymbol{\nabla}_{x_i} \Psi_N \right] + \boldsymbol{\nabla}_{p_i} \cdot \left[-\dot{\mathbf{p}}(\mathbf{x}_i, \mathbf{p}_i; \Xi)\Psi_N + d_r \boldsymbol{\nabla}_{p_i} \Psi_N \right] \right\}, \tag{3.1}$$

governing the joint probability density function (p.d.f.) Ψ_N for the N-particle configuration Ξ. The high-dimensional N-particle Fokker–Planck equation (3.1) is intractable without appropriate reduction, which we shall demonstrate in the following section, but writing (3.1) down explicitly serves as a reminder that this is the common starting point for most coarse-grained continuum models [18,35,36]. For pedagogical simplicity, in this article, we will assume all particles are identical, allowing for the removal of the subscript i from particle parameters such as V^c, $\mathbf{V}^F$, β and α. However, it should be stressed that, in reality, parameters such as V^c can have a large variation among particles, which can significantly impact their collective dynamics [37].

(a) Averaging towards a one-particle equation

Our goal now is to obtain a macroscopic model for the one-particle density by reducing (3.1) through a series of approximations. Let us first define the notation for the averaging operator. For any function $\star(\Xi)$ of the configuration Ξ, the ensemble average over all particle configurations except for the first k particles is defined as

$$\langle \star \rangle_k = \int_{\Upsilon^{N-k}} \star(\Xi)\Psi_N d\boldsymbol{\xi}_{k+1} ... d\boldsymbol{\xi}_N, \tag{3.2}$$

where $\Xi \in \Upsilon^{N-k}$ is the domain of all allowed configurations for the $(k+1)$-th to N-th particles. The joint p.d.f. for the first k-particles is thus defined by putting $\star = 1$, $\Psi_k(\boldsymbol{\xi}_1, ..., \boldsymbol{\xi}_k, t) = \langle 1 \rangle_k = \int_{\Upsilon^{N-k}} \Psi_N d\boldsymbol{\xi}_{k+1} ... d\boldsymbol{\xi}_N$. For example, with $\star = 1$, putting $k = 0$ recovers the normalization constant $\langle 1 \rangle_0$, which we set to unity, while putting $k = 1$ provides the 1-particle p.d.f., for which the evolution equation can be obtained by performing the same $\langle \star \rangle_1$ operation on (3.1), yielding

$$\begin{aligned} \partial_t \Psi_1(\mathbf{x}_1, \mathbf{p}_1, t) = {} & \boldsymbol{\nabla}_{x_1} \cdot \left[-\langle \mathbf{u} \rangle_1(\mathbf{x}_1, t) - \left(V^c \mathbf{p}_1 + \mathbf{V}^F(\mathbf{p}_1) \right) \Psi_1 + D_T \boldsymbol{\nabla}_{x_1} \Psi_1 \right] \\ & + \boldsymbol{\nabla}_{p_1} \cdot \left[-\left(\boldsymbol{\Omega}_{\text{jeff}}(\langle \mathbf{u} \rangle_1, \mathbf{p}_1) + \beta \left(\mathbf{p}_1 \times \hat{\mathbf{k}} \right) \Psi_1 \right) \times \mathbf{p}_1 + d_r \boldsymbol{\nabla}_{p_1} \Psi_1 \right], \end{aligned} \tag{3.3}$$

[1]The removal of the sum of external forces is the equivalent of renormalization [33], in which a net flow condition is enforced by balancing the total external net forces on the system with the pressure gradient. Under our point particle approximation, the particle has no volume, and, therefore, there is no exclusion of regions of overlap that generate extra hindrance to sedimentation. Instead, the sum of external forces simply modifies the pressure gradient [33]

where the averaged velocity $\langle \mathbf{u} \rangle_1(\mathbf{x_1}, \mathbf{t})$ is defined as

$$\langle \mathbf{u} \rangle_1(\mathbf{x_1}, t) = \int_{\Upsilon^{N-1}} \mathbf{u}(\mathbf{x}_1, t; \Xi \backslash \boldsymbol{\xi}_1) \Psi_N d\boldsymbol{\xi}_2 ... d\boldsymbol{\xi}_N = \int_{\Upsilon^{N-1}} \sum_{j=2}^{N} \mathbf{u}_j(\mathbf{x}_1, t; \boldsymbol{\xi}_j) \Psi_N d\boldsymbol{\xi}_2 ... d\boldsymbol{\xi}_N. \tag{3.4}$$

Since the particles are approximated as flow-independent point forces ($\mathbf{F}_j$ a constant vector) and dipoles ($\mathtt{M}_j = \sigma_j \mathbf{p}_j \mathbf{p}_j$), there are no three-way particle interactions. Therefore, under the assumption that the particles are also indistinguishable, we can further simplify the N-particle integral into a 2-particle integral,

$$\langle \mathbf{u} \rangle_1(\mathbf{x}_1, t) = (N-1) \Psi_1(\boldsymbol{\xi}_1, t) \int_{\Upsilon^1} \mathbf{u}_2(\mathbf{x}_1, t; \boldsymbol{\xi}_2) \Psi_{2|1}(\boldsymbol{\xi}_2, t | \boldsymbol{\xi}_1) d\boldsymbol{\xi}_2, \tag{3.5}$$

where $\Psi_{2|1} = \Psi_2 / \Psi_1$ is the conditional p.d.f. of ξ_2 given the configuration of the first particle ξ_1. Therefore, defining the average flow (and the corresponding pressure) due to the presence of the other particle as $\tilde{\mathbf{u}}(\mathbf{x}, t) = (N-1) \int_{\Upsilon^1} \mathbf{u}_2(\mathbf{x}, t; \boldsymbol{\xi}_2) \Psi_{2|1}(\boldsymbol{\xi}_2, t | \boldsymbol{\xi}_1) d\boldsymbol{\xi}_2$ (and $\tilde{q}$), we have

$$\begin{aligned} \partial_t \Psi_1 \left(\mathbf{x}_1, \mathbf{p}_1, t \right) = & \boldsymbol{\nabla}_{x_1} \cdot \left[- \left(\tilde{\mathbf{u}} \left(\mathbf{x}_1, t \right) + V^c \mathbf{p}_1 + \mathbf{V}^F \left(\mathbf{p}_1 \right) \right) \Psi_1 + D_T \boldsymbol{\nabla}_{x_1} \Psi_1 \right] \\ & + \boldsymbol{\nabla}_{p_1} \cdot \left[- \left(\boldsymbol{\Omega}_{\text{jeff}} \left(\tilde{\mathbf{u}} \left(\mathbf{x}_1, t \right), \mathbf{p}_1 \right) + \beta \mathbf{p}_1 \times \hat{\mathbf{k}} \right) \times \mathbf{p}_1 \Psi_1 + d_r \boldsymbol{\nabla}_{p_1} \Psi_1 \right] \end{aligned} \tag{3.6}$$

and

$$\mathbf{0} = -\boldsymbol{\nabla}_x \tilde{q} + \mu \nabla_x^2 \tilde{\mathbf{u}} + (N-1) \left(\int_{p_2} (\mathbf{F}_2 + \mathtt{M}_2 \cdot \boldsymbol{\nabla}_x) \Psi_{2|1} d\mathbf{p}_2 - \frac{\mathbf{F}_2}{V} \right), \quad \boldsymbol{\nabla}_x \cdot \tilde{\mathbf{u}} = 0. \tag{3.7}$$

In essence, the equations above summarize the basis of a typical continuum model for the active suspensions, which are also represented in figures figure 1c–f. Now, computing Ψ_1 requires $\Psi_{2|1}(\boldsymbol{\xi}_2, t | \boldsymbol{\xi}_1)$. This can be found by repeating the above procedures using $\langle \star \rangle_2$ in place of $\langle \star \rangle_1$ to get the 2-particle equation for $\Psi_2(\boldsymbol{\xi}_1, \boldsymbol{\xi}_2, t)$, but the corresponding flow equation will require Ψ_3, and so on, forming a hierarchy analogous to the BBGKY hierarchy for Hamiltonian systems [35,36]. To close this reduction to a 1-particle equation requires further assumptions or approximations. In the following section, we will discuss the simplest way to close the problem—the mean-field approximation. A more general discussion on other potential closure relationships will be discussed at the end of the work.

(b) Mean-field approximation

In the dilute limit $\phi \to 0$, particles do not interact frequently or strongly, allowing the probabilities of two particles' configurations to be approximated as independent, i.e. $\Psi_2(\boldsymbol{\xi}_1, \boldsymbol{\xi}_2, t) \approx \Psi_1(\boldsymbol{\xi}_1, t) \Psi_1(\boldsymbol{\xi}_2, t)$ and, consequently, $\Psi_{2|1}(\boldsymbol{\xi}_1, \boldsymbol{\xi}_2, t) \approx \Psi_1(\boldsymbol{\xi}_1, t)$. Substituting the approximation into ((3.6) and (3.7)) gives rise to the DSS model (cf. equations (1)–(5) in [14])

$$\begin{aligned} \partial_t \Psi_1 \left(\mathbf{x}_1, \mathbf{p}_1, t \right) = & \boldsymbol{\nabla}_{x_1} \cdot \left[- \left(\tilde{\mathbf{u}} \left(\mathbf{x}_1, t \right) + V^c \mathbf{p}_1 + \mathbf{V}^F \left(\mathbf{p}_1 \right) \right) \Psi_1 + D_T \boldsymbol{\nabla}_{x_1} \Psi_1 \right] \\ & + \boldsymbol{\nabla}_{p_1} \cdot \left[- \left(\boldsymbol{\Omega}_{\text{jeff}} \left(\tilde{\mathbf{u}} \left(\mathbf{x}_1, t \right), \mathbf{p}_1 \right) + \beta \mathbf{p}_1 \times \hat{\mathbf{k}} \right) \times \mathbf{p}_1 \Psi_1 + d_r \boldsymbol{\nabla}_{p_1} \Psi_1 \right] \end{aligned} \tag{3.8}$$

and

$$\mathbf{0} = -\boldsymbol{\nabla}_x \tilde{q} + \mu \nabla_x^2 \tilde{\mathbf{u}} + (N-1) \left(\int_{p_1} \mathbf{F}_1 \Psi_1 + \boldsymbol{\nabla}_x \cdot (\mathtt{M}_1 \Psi_1) d\mathbf{p}_1 - \frac{\mathbf{F}_1}{V} \right), \quad \boldsymbol{\nabla}_x \cdot \tilde{\mathbf{u}} = 0. \tag{3.9}$$

Note the subtle difference in the subscripts between (3.7) and (3.9) and the new definition of $\tilde{\mathbf{u}}(\mathbf{x}, t) = (N-1) \int_{\Upsilon^1} \mathbf{u}_1(\mathbf{x}, t; \boldsymbol{\xi}_1) \Psi_1(\boldsymbol{\xi}_1, t | \boldsymbol{\xi}_1) d\boldsymbol{\xi}_1$ (and the corresponding $\tilde{q}$). They are the results of the independence assumption under the dilute approximation, which removes the dependence on the configurations of other particles and effectively closes the BBGKY hierarchy. In addition to the independence assumption above, here we also summarize all the other assumptions made so far. (1) Particles are inertia-less and small enough to be considered Stokesian. Their overdamped trajectories can be explicitly written out. (2) Particles are indistinguishable to allow for the simplification

from the N-particle integral (3.4) to the 2-particle integral (3.5). (3) Particle disturbances are represented by the first two terms in the multipole expansion, dependent only on the particle's own configuration and not the others (i.e. flow-independent); all hydrodynamic interactions are approximated as one-way, which is accurate up to $\mathcal{O}(\phi^{1/3})$ [38]. (4) Near-field interactions between particles are neglected; there are no repulsive, lubrication or steric forces between the particles and, therefore, no volume exclusion. The whole domain is accessible to each particle. (5) There is no correlation between the distribution of any two particles, leading to $\Psi_{2|1}(\boldsymbol{\xi}_2, t|\boldsymbol{\xi}_1) \approx \Psi_1(\boldsymbol{\xi}_2, t)$. The lack of domain exclusion (4) implies the result is only $\mathcal{O}(1)$ accurate in ϕ [33]; the DSS model is accurate only when $\phi \to 0$. Later in §4a, we will show how the assumption can lead to unphysical artefacts.

Also, note that the equivalent procedure from (2.8) to (3.9) with the full Navier–Stokes equation instead of the Stokes equation will *not* result in a Navier–Stokes extension to (3.9) in the form of

$$\rho_f(\partial_t \tilde{\mathbf{u}} + \tilde{\mathbf{u}} \cdot \boldsymbol{\nabla}_x \tilde{\mathbf{u}}) = -\boldsymbol{\nabla}_x \tilde{q} + \mu \nabla_x^2 \tilde{\mathbf{u}} + (N-1)\left(\int_{p_1} \mathbf{F}_1 \Psi_1 + \boldsymbol{\nabla}_x \cdot (\mathtt{M}_1 \Psi_1) d\mathbf{p}_1 - \frac{\mathbf{F}_1}{V}\right). \tag{3.10}$$

This is because the ensemble averaging of velocity $\langle \mathbf{u} \rangle_1(\mathbf{x_1}, t)$ in (3.4) implicitly requires a linear superposition of the governing equation of the flow, which is not supported by the nonlinearity in the Navier–Stokes equation. Therefore, despite its common usage in modelling nonlinear phenomena such as bioconvection (e.g. equation (1.2) in [6] and equation (4.4) in [7]), the derivation of this equation is not formally established here and should be treated with caution. Nonetheless, in the absence of a better model, (3.10) remains a widely accepted empirical model for nonlinear phenomena in dilute active suspensions.

Lastly, we should emphasize that the mean field may not always account for all spatio-temporal correlations in the system. As mentioned in §1, in bacterial turbulence, the statistical correlation between two points can still show the presence of large vortices before the onset of instability [16], where the mean field is supposedly isotropic and homogeneous [14]. To capture such correlation, one will have to go beyond the mean field in the BBGKY hierarchy and explicitly calculate the correlation functions [17].

(c) Reducing the high-dimensional Fokker–Planck equation

While the DSS model is a good approximation for dilute suspensions and can be rigorously derived from microscopic dynamics, in practice, (3.6) is rarely numerically solved in three-dimensional systems due to its high dimensionality [39,40].

To overcome this limitation, one approach is to take successive orientational moments of (3.6), which yield a set of 'hydrodynamic' equations for particle density, polar order and nematic order [26,41] that also resemble the equivalent phenomenological models [25]. However, this approach gives rise to a hierarchy of equations that require either an *ad hoc* closure [42–44] or an asymptotic approximation [45] of the higher-order moments [46, §2.7.1]. A notable closure model is the Bingham closure, which approximates the distribution to take the form of a Bingham distribution [47]. It has been shown to be both computationally attractive while retaining the essential physics, such as the evolution of system entropy and the trace condition on the nematic order [44]. On the other hand, since fluctuations were found to be crucial in phenomena like bacterial turbulence, some [19] have also proposed that closure takes into account these fluctuations.

The second approach involves asymptotically separating the rapid orientational dynamics from the slower translational dynamics, assuming that the orientational distribution relaxes to a quasi-steady state much more quickly than the translational dynamics. To this end, the GTD theory has been employed to derive the effective drift and dispersion of tactic particles in simple linear flows [11,12]. However, the particle density equation obtained using GTD in one flow is not intended to be applicable to other flows. Furthermore, inappropriate application of GTD may result in inaccurate estimations of particle density [48] or singularities in the effective diffusivity

[49]. To address this issue, Fung *et al.* [50] proposed the local approximation model. Similar to Pedley & Kessler's model [7], this method gives effective drift and dispersion as functions of the local flow field and particle taxes instead of the global flow field like GTD. It was demonstrated to be accurate in predicting shear trapping phenomena [51] and requires no knowledge of the global flow field, making it more generalizable than the GTD [48]. However, the local approximation model is still limited to cases where orientational dynamics are fast and has limited applicability to fast unsteady flows.

4. Outstanding challenges in continuum modelling

(a) Volume exclusion and near-field interactions between particles

An underlying assumption in the derivation above is that the particles are treated as point particles, meaning that the volume fraction $\phi \to 0$. Occasionally, this assumption can result in unphysical outcomes as the model does not account for volume exclusion effects. To illustrate, let us consider the example of gyrotactic focusing of bottom-heavy ($\beta \propto L > 0$, $\hat{\mathbf{k}} \parallel -\mathbf{g}$), negatively-buoyant ($\Delta\rho > 0$) motile microorganisms such as *Chlamydomonas augustae* (née *nivalis*) [5,7]. The DSS model was applied to this suspension in a recent work [52], which revealed a surprising equivalence between the DSS model for gyrotactic focusing and the Keller–Segel model for autochemotaxis. Similar to the well-known chemotactic collapse in the Keller–Segel model [53], the steady-state velocity and particle density in the DSS model also tend to infinity locally in three-dimensional systems. The same singularity was also found when applying the DSS model to the sedimentation of spheroids [52] and chemotactically active immotile particles on gas–fluid interfaces [54]. Although the aggregation of particles does corroborate experimental observations, the unrealistic blow-up of local particle density shows the importance of incorporating the volume exclusion effect.

The finite volume of particles can necessitate multiple corrections: (1) The passive advection $\mathbf{u}(x_i, t, \Xi \backslash \boldsymbol{\xi}_i)$ should be corrected using the Faxén law to account for variation in the flow at the length scale of the particle. (2a) The naive superposition of multipole expansions of Green's function as a representation of disturbance by each particle is no longer strictly valid, but remains a good approximation by the method of reflections. The finite size of particles implies that each particle will exert an extra stresslet depending on the local strain rate due to background flow and disturbance flow from other particles. (2b) Since this stresslet depends on the configuration of other particles, three or more particle interactions become finite (but small), and the step from (3.4) to (3.5) is no longer exact. (3) Volume exclusion implies that the domain of $\Psi_{2|1}$ has impenetrable regions, which can induce significant corrections. For example, in the sedimentation problem [33], it is the exclusion of this region during renormalization that induces a correction to the average sedimentation speed, which is -6.55ϕ including the Faxén correction. (4) There is a non-zero chance that particles will come into close contact with each other. When their surfaces are at a distance $h \lesssim a$, the far-field multipole expansion of the disturbance flow is no longer valid, and the flow field around two particles must be calculated explicitly [55,56]. (5) As a result of the near-field interactions, the pairwise correlation $\Psi_{2|1}$ is likely not well approximated by $\Psi_{2|1} \approx \Psi_1(\boldsymbol{\xi}_2, t)$, and the closure relationship between $\Psi_{2|1}$ and Ψ_1 near particle 1 must be re-examined.

Methodologies to account for (1–3) are well-established [33] if the pair correlation $\Psi_{2|1}$ is known, but the exact physics of the near-field interactions (4) is still an active area of research even in passive suspensions [57] due to lubrication breakdown [58]. Moreover, past work on passive suspensions showed that the approximation of $\Psi_{2|1}$ in (5) is highly sensitive to the exact near-field interactions in some problems due to the singular nature of pairwise trajectories in Stokes flow [59]. As a result, macroscopic properties like the bulk stress in the sheared passive suspension are hard to predict and are highly sensitive to the near-field interactions governed by the geometry and surface properties of the particles [59]. For self-propelling particles such as swimming microorganisms and artificial microswimmers, deriving macroscopic models that

account for the finite volume will be more challenging, as the near-field interactions will likely depend on the specific propulsion mechanics and microscale flow around the particles. While exact analytical results are available for simple spherical squirmers [56], there is no general theory to calculate near-field interactions between arbitrary particles other than employing prohibitive numerical methods. Moreover, it is expected that real biological microswimmers will have a wide variety of shapes and sizes, making the calculation of near-field interactions intractable. Therefore, it remains an open challenge to derive a general framework that can include complex and wide variations of two-particle interactions in a coarse-grained model.

(b) Overcoming the closure problem in many-body systems

The above discussion focuses on pairwise interactions, which, when resolved, can improve the model accuracy at finite volume fractions. To extend the approximation to higher ϕ, many-body interactions should be considered [59]. However, as demonstrated by the derivation of (3.7), the consideration of N-body interactions in equation for Ψ_N always requires information from Ψ_{N+1}. This is the BBGKY hierarchy, which is a fundamental challenge in many-body systems. While there are many approaches to overcome this closure problem, here we present two recent developments in neighbouring fields that may offer new opportunities in addressing the problem in the context of active suspensions. Reviews by [35,36,60] offer an introduction to alternative approaches.

(i) Dynamical density functional theory

Density functional theory (DFT) is a powerful tool in statistical mechanics that is used to write down the equilibrium description of an interacting particle system as a one-particle density that minimizes the free energy functional. It determines the distribution correlation between particles by using an equilibrium argument, effectively closing the BBGKY hierarchy. In dynamical DFT (DDFT), the idea of solving distribution correlation using free energy functionals is extended to dynamically evolving systems, where the pairwise correlation in the dynamically evolving non-equilibrium system is approximated to be the same as that of the equilibrium system with the same one-body density. This heuristic approximation is known as the adiabatic approximation. DDFT has been used to study the dynamics of hydrodynamically interacting particles [61], 'dry' active Brownian particles [62] and, most notably here, for microswimmers (i.e. suspended active particles) [63]. A caveat of the theory, however, is that for the adiabatic approximation to remain valid, the dynamics of the system must evolve close to equilibrium, which is particularly problematic for active particles where the system is driven far from equilibrium by the activity of the particles. Therefore, the approach may be limited to systems with weak activity. The review by [60] provides a good summary of the method, its limitations and a comprehensive list of applications of theory in various fields.

(ii) Matched asymptotic method for excluded-volume active particles

Bruna & Chapman [64] demonstrated a novel matched asymptotic technique to account for the excluded-volume effect when reducing the N-particle Fokker–Planck equation into a one-particle equation for a system of interacting hard-sphere particles. Focusing on the interaction between two spheres, Bruna & Chapman separated the inner region near the first sphere, where the probabilities of two spheres are correlated, from the outer region, where the two spheres are uncorrelated, via asymptotic expansion in the limit of small volume fractions. Then, by matching the inner and outer solutions, Bruna derived a one-particle equation that corrects the drift and diffusion terms to first order in ϕ. Recently, Bruna extended the method to active Brownian particles [35] under the assumption that the particles only interact through a hard-core potential. It remains to be seen if the method can be extended to suspended active particles, where both long-range hydrodynamic interactions and short-range lubrication forces are present. A challenge in extending

the method to suspended particles is that hydrodynamic interactions are long-range, in contrast to the short-range hard-core potential of previous work.

(c) Prescribing physically relevant boundary conditions

A further challenge in developing continuum models for active particles is prescribing a mathematically well-posed and physically correct boundary condition that captures the interaction between the particles and the boundary. Active particles are well known to exhibit unique interactions with the boundary. Observations include bacteria swimming in circles [65], attraction to or repulsion from the boundary [66], upstream swimming near boundaries [67,68] and biofilm formation [69]. These phenomena are primarily related to the existence of a plane boundary. Observations diversify even further if one considers constrictions [70,71], the geometric complexity of the boundaries [72] and/or behavioural change of the particle [73]. Several reviews are available summarizing such findings [74–76].

(i) Individual interactions with the boundary

The existence of a boundary brings three kinds of interactions into consideration: hydrodynamic, steric and behavioural. We denote contact-free interactions via the fluid medium as hydrodynamic, the contact-driven interactions as steric and any biological response near the boundary as behavioural. Much focus has been given to the debate on whether hydrodynamic or steric interactions dominate the entrapment of pusher particles such as bacteria near the boundary [66,77–81], as both hydrodynamic and steric interactions can give rise to the accumulation of particles near the boundary. Recent experiments [29,82–85] have shown a more nuanced picture where, depending on the exact geometry and swimming mechanisms of the particle, both hydrodynamic and steric interactions can play a role in the entrapment or scattering of particles at the boundary. However, one should also note the potential for behavioural changes of microorganisms near the boundary (e.g. [73]), which can become dominant and further complicate the picture. Here, we shall not discuss how these mechanisms give rise to different phenomenology, but merely highlight how one can account for these effects in a continuum model.

Individually, hydrodynamic interactions with the boundary can be represented as corrections to the translational and rotational dynamics that depend on the position and orientation relative to the boundary. For example, a pusher ($\sigma > 0$) is attracted to a no-slip wall and will reorient to swim parallel to the wall due to the reflected disturbance flow from the axisymmetric force dipole $S = \sigma \mathbf{pp}$ [66]. Surprisingly, the far-field representation of the particle (2.2) is accurate enough to capture the essential boundary interactions even when the distance between the particle and the boundary is a fraction of the particle length scale [78]. Further corrections can be built upon this framework, such as time dependency due to flagella undulation [86] and noise-induced drift due to wall-induced spatial gradient of particle motility [87]. We refer the reader to [27, ch. 11] for more details on hydrodynamic interactions at the boundaries.

Regardless of complexity, the hydrodynamic interactions with the boundary can always be represented by a correction to ((2.3)–(2.5)) if particles are assumed to only affect themselves. Alternatively, extra disturbance in the form of (2.2) from the image of the particle can be added to the coarse-graining framework in the previous sections if hydrodynamic interactions between particles via reflection of the wall are of concern. Either way, one can incorporate hydrodynamic interactions with the boundary in a mean-field continuum model simply by adding the correction terms in either (2.2) or ((2.3)–(2.5)) and follow the coarse-graining procedure laid out in the previous section. Nonetheless, continuum modelling of hydrodynamically interacting particles near the wall remains sporadic [88].

As for steric interactions, on an individual level, the common approach is to empirically add a repulsive force from a wall potential [79,89,90]. While some authors have opted for smooth approximations to potential functions that are easier to treat analytically [29], the physical origin

of such contact forces merits more attention [91]. Although the reorientation of active particles near walls is often attributed to hydrodynamics, it should be noted that a contact force from the boundary can also cause particle reorientation if the particle is not spherical and the force acts off-centre [82,85]. Much like hydrodynamic interactions, the effects of repulsive forces can be easily accounted for by adding correction terms to ((2.3)–(2.5)).

(ii) Boundary conditions for the Fokker–Planck equation at different scales

When particles are stochastic, volume exclusion further restrains the stochastic force from pushing the particles through the boundary, which requires further treatment in both individual-based and continuum models. At the individual and microscopic level, the conventional method to prevent particles experiencing thermal Brownian motion from crossing the boundary is to reflect their positions about the boundary but not their orientations [92,93].[2] This reflection ensures that no particle flux passes through the boundary. At the continuum level, this treatment is equivalent to the no-flux Robin boundary condition [80,81,94], given by

$$D_T \frac{\partial \Psi}{\partial \mathbf{n}} = V_s \mathbf{p} \cdot \mathbf{n} \Psi, \tag{4.1}$$

where $\mathbf{n}$ is the normal vector to the boundary. Since the balance between the swimming and diffusive flux is enforced at each $\mathbf{p}$, (4.1) will lead to a boundary layer of polarized particles accumulating near the wall with a thickness scaling with D_T. Some authors [80,81,95] argue that the near-wall accumulation is in qualitative agreement with experimental observations [77,96], although further work is required to establish this conclusively. Others interpret the boundary condition as unrealistic [97] and over-restrictive, as (4.1) prescribes that particles do not reorient upon contacting the wall. Also, for many realistic active particles, D_T is vanishingly small, which may lead to an impractical boundary layer thickness or ill condition in (4.1). Here, it is important to note that D_T does not represent the thermal diffusivity because active particles of μm size are too large to experience significant translational Brownian motion (cf. §2b). Instead, it is exploited as a 'catch-all' model for any physical, stochastic or biological behaviour that is not captured in (2.3)–(2.5). The question of how these behaviours change upon contact with the boundary remains unanswered, but it is probable that simple reflection off the wall without reorientation would be an oversimplification. Nonetheless, in theoretical studies of reorientational dynamics in stochastic point/spherical particles near a boundary due to hydrodynamic and contact forces, it is still reasonable to use the reflection or the corresponding Robin boundary condition (4.1) to keep particles from crossing the boundary, as they are mathematically consistent with the bulk and do not introduce any additional reorientation dynamics. As for non-spherical particles, the admissible position of the centre of the particle constrained by the boundary depends on the particle shape and $\mathbf{p}$, thereby creating a complex boundary geometry in the $\mathbf{x} - \mathbf{p}$ space. To this end, Chen & Thiffeault [72] proposed a mapping method to specify the boundary geometry according to the particle shape.

While the above-mentioned boundary conditions hold theoretical significance for studying the microscopic dynamics near the wall, their applications in confined macroscopic systems are often impractical due to the large separation of scales between the microscopic dynamics near the wall and the bulk scale dynamics. Moreover, modelling realistic biological swimmers with the above-mentioned methods often proves too complex. For example, real biological swimmers have complex time-varying geometry, like beating cilia or flagella, to generate propulsion, deeming Chen & Thiffeault's method challenging to apply. In other cases, behavioural changes near the

[2]The word 'reflecting' boundary is taken from the convention [93] on modelling random walks close to a boundary, where a random walker is reflected about the boundary when it crosses, while keeping the configuration in the dimensions orthogonal to the wall direction unchanged. To avoid confusion with boundaries that reflect both the position and orientation of the particle like a pin-ball, we will use the term 'specularly reflecting' boundary to refer to the latter case where both $\mathbf{p}$ and position in the wall-normal direction are reflected.

boundary, such as the sharp turn of algae [73] and the change in phenotype of biofilm-forming bacteria [69], dominate over other physical interactions.

Considering the challenges to accurately model boundary interactions, a more feasible way to represent them at the bulk scale may be to encompass all of the above-mentioned effects in an empirical boundary condition inferred from statistical data of particle scattering or entrapment at the boundary [78,82,84]. For example, the sharp turnaround of algae [73,82] motivates a specular reflection boundary condition [49,98],

$$\Psi(\mathbf{x}, \mathbf{p}, t) = \Psi(\mathbf{x}, \mathbf{p} + 2(\mathbf{p} \cdot \mathbf{n})\mathbf{n}, t), \tag{4.2}$$

where particles bounce off the wall like a billiard ball with the angle of reflection equal to the angle of incidence. This condition is popular among the recent work in continuum models [94,99,100] due to its ease of implementation and admission to simple solutions such as a uniform steady solution [81], but it is likely an oversimplification of the real scattering correlation between incoming and outgoing angles, which often shows particles emerging at a fixed angle irrespective of the incoming angle [78,82]. In other cases, particles may emerge from the wall with a wide distribution of orientation [84], which motivates a uniform random reflection condition in the limiting case. The entrapment of some bacteria on the surface and their eventual formation of biofilms may motivate an absorbing boundary condition. The effects of these possible limiting boundary conditions on the bulk were explored in [97] in the context of a channel flow where the absorbing boundary is simply represented by $\Psi = 0$ on the boundaries for all orientations.

(iii) Boundary conditions for the particle density equation

As mentioned in §3c, the equation for the probability density $\Psi(\mathbf{x}, \mathbf{p}, t)$ in $\mathbf{x}$ and $\mathbf{p}$ can be further reduced into an equation for the particle density $n(\mathbf{x}, t)$. The most basic boundary condition to apply in this case is the no-flux condition, where the advective flux due to motility must balance the diffusive flux, such that

$$\mathbf{n} \cdot (\bar{\mathbf{V}} n - \bar{D} \cdot \boldsymbol{\nabla}_x n) = 0 \quad \text{on} \quad \Omega. \tag{4.3}$$

Here, $\bar{\mathbf{V}}$ and $\bar{D}$ can be modelled using the effective drift and diffusivity derived from the reduction in the bulk (§3c), but using the bulk values would be an oversimplification, as particle trajectories are modified by boundaries. However, given the aforementioned difficulties in accounting for the exact interactions between the particles and the boundary, there is little work on how $\bar{\mathbf{V}}$ and $\bar{D}$ should be modified by the boundaries.

Besides the no-flux boundary, it is also possible to have an absorbing boundary at the macroscopic scale, given that particles can be trapped at the boundary at the microscopic scale physically or biologically. The condition has practical relevance in terms of biofilm formation, a phenomenon detrimental to many systems such as bioreactors and catheters [101]. This will require the boundary conditions to be updated to the form

$$\mathbf{n} \cdot (\bar{\mathbf{V}} n - \bar{D} \cdot \boldsymbol{\nabla}_x n) = -\gamma n \quad \text{on} \quad \Omega, \tag{4.4}$$

where γ appears as an absorption coefficient. This condition renders the classical methods founded upon no-flux boundaries cumbersome to manipulate [102], requiring different approaches [100,103,104].

5. Conclusion and outlook

In this work, we have presented the systematic derivation of a mean-field model for dilute active suspensions from the microscopic dynamics of active particles and their far-field hydrodynamic interactions. In particular, we have clarified the approximations required to reduce the N-particle Fokker–Planck equation (3.1) to the one-particle mean-field equation (the DSS model). The approximations assume that suspensions are dilute ($\phi \to 0$), and the probability of each particle

configuration is independent of the others ($\Psi_{2|1} \approx \Psi_1$). However, as the mean-field model does not account for volume exclusion between particles, it can lead to unphysical artefacts, such as particle density singularities when modelling gyrotactic focusing [52]. Moreover, recent work on bacterial turbulence has shown that the mean-field model is not sufficient for describing the full dynamics of the system [16]. Even when the mean field is isotropic and homogeneous, fluctuations may be correlated, leading to the emergence of bacterial turbulence [17].

We also briefly reviewed the approximation techniques for further reducing the high-dimensional one-particle Fokker–Planck equation. One strategy, popular among soft matter physicists, led to the 'hydrodynamic' equations for self-propelling particles [26,41]. Others provide an effective transport equation for particle density, assuming that the orientational distribution rapidly converges to a quasi-steady equilibrium [11,12,50]. However, one should exercise caution when interpreting the resulting transport model, as some methods, such as the GTD model, are based on the restrictive assumption of homogeneity in the global flow field. Fortunately, with the advent of increasing computational power, direct numerical simulation of the Fokker–Planck equation may soon become practical, with recent methods [50,94,99] tackling four of the five dimensions in the equation.

To further develop the coarse-graining framework into a mature and quantitatively accurate model for active suspensions, there remain several major challenges. Firstly, recent results on phenomena such as gyrotactic focusing suggest that one should account for the finite volume of the particles and their near-field interactions [52]. Although some analytical treatments for near-field interactions between active particles in simple geometries exist [56], most studies on such interactions rely on well-established numerical methodologies (e.g. [105]). There is also a trend towards higher fidelity in near-field models, where particle geometries are increasingly complex and the flow increasingly intractable. Therefore, developing coarse-graining frameworks that can incorporate the numerical results of near-field interactions is a pressing challenge.

Secondly, there needs to be more development beyond the current mean-field model, which the field has relied on since the early 2000s [11,12]. To include the volume exclusion effect and better account for two-particle correlations, one could borrow techniques from the classical literature [33,59] on passive suspensions and extend them to active suspensions. Further improvements may be made by considering three-body interactions and beyond, using the methods in §2b. Alternatively, the neighbouring fields of plasma physics and self-gravitating matter may also offer valuable lessons in modelling many-body systems with long-range interactions.

Finally, modelling particles close to boundaries remains a significant challenge. The physical interactions between individual particles and the boundary have received a lot of attention [29,77–85], but the continuum modelling of these interactions is sparse. As the interactions occur at the particle length scale, the particle density can form a microscale boundary layer. To simplify computations, it might be necessary to further homogenize the boundary interactions into an effective boundary condition at the macroscopic scale. Also, as biological microswimmers can alter their behaviour close to the boundary [73], it may be more practical to adopt a data-centric approach to the creation of macroscopic effective boundary conditions. Rather than establishing the boundary interactions from physical principles, statistical data on particle scattering or entrapment at the boundary [78,82,84] can be used to infer empirical boundary conditions for macroscopic continuum models.

Aside from these key challenges, there are other important outstanding questions. For example, biological swimmers are typically propelled by relatively long rotating or beating flagella, but these may interact hydrodynamically and synchronize when in close proximity [106]. How does one account for the effect of synchronization and indeed the complex flagellum-wall interactions in a continuum model? In addition to the noise in orientation d_r, bacteria also tumble randomly. How does run-and-tumble motion, or more generally taxes, change near the boundary, and how does one coarse-grain such a change in behaviour? In realistic microswimmer suspensions, swimming speed and gyrotactic strength can vary widely in the population. How does polydispersity

influence their collective dynamics [34]? These questions present additional challenges to the coarse-graining framework described in this work.

Data accessibility. This article has no additional data.

Declaration of AI use. We have not used AI-assisted technologies in creating this article.

Authors' contributions. L.F.: conceptualization, funding acquisition, investigation, methodology, project administration, supervision, writing—original draft, writing—review and editing; H.O.C.: investigation, writing—original draft, writing—review and editing; M.B.: supervision, writing—review and editing.

All authors gave final approval for publication and agreed to be held accountable for the work performed therein.

Conflict of interests. We declare we have no competing interests.

Funding. L.F. is supported by the Research Fellowship from Peterhouse, Cambridge.

Acknowledgements. We gratefully acknowledge E.J. Hinch for his guidance on coarse-graining, P.H. Htet for his assistance in preparing the discussion on wall interactions, E. Yeo, W. Ridgway, W. Liao and M. te Vrugt for their helpful feedback on the manuscript.

References

1. Wang Q, Zhang T. 2010 Review of mathematical models for biofilms. *Solid State Commun.* **150**, 1009–1022. (doi:10.1016/j.ssc.2010.01.021)
2. McGillicuddy DJ, Franks PJS. 2019 Models of plankton patchiness. In *Encyclopedia of ocean sciences*, pp. 536–546, 3rd edn. Oxford, UK: Elsevier. (doi:10.1016/B978-0-12-409548-9.11610-0)
3. Bees MA, Croze OA. 2014 Mathematics for streamlined biofuel production from unicellular algae. *Biofuels* **5**, 53–65. (doi:10.4155/bfs.13.66)
4. Childress S, Levandowsky M, Spiegel EA. 1975 Pattern formation in a suspension of swimming microorganisms: equations and stability theory. *J. Fluid Mech.* **69**, 591–613. (doi:10.1017/S0022112075001577)
5. Kessler JO. 1986 Individual and collective fluid dynamics of swimming cells. *J. Fluid Mech.* **173**, 191–205. (doi:10.1017/S0022112086001131)
6. Pedley TJ, Kessler JO. 1990 A new continuum model for suspensions of gyrotactic microorganisms. *J. Fluid Mech.* **212**, 155–182. (doi:10.1017/s0022112090001914)
7. Pedley T. 1992 Hydrodynamic phenomena in suspensions of swimming microorganisms. *Annu. Rev. Fluid Mech.* **24**, 313–358. (doi:10.1146/annurev.fluid.24.1.313)
8. Hinch EJ, Leal LG. 1972 Note on the rheology of a dilute suspension of dipolar spheres with weak Brownian couples. *J. Fluid Mech.* **56**, 803–813. (doi:10.1017/S0022112072002666)
9. Brenner H. 1974 Rheology of a dilute suspension of axisymmetric Brownian particles. *Int. J. Multiph. Flow* **1**, 195–341. (doi:10.1016/0301-9322(74)90018-4)
10. Berg HC. *Random walks in biology*. Princeton, NJ, USA: Princeton University Press. (doi:10.2307/j.ctv7r40w6)
11. Hill NA, Bees MA. 2002 Taylor dispersion of gyrotactic swimming micro-organisms in a linear flow. *Phys. Fluids* **14**, 2598–2605. (doi:10.1063/1.1458003)
12. Manela A, Frankel I. 2003 Generalized Taylor dispersion in suspensions of gyrotactic swimming micro-organisms. *J. Fluid Mech.* **490**, 99–127. (doi:10.1017/s0022112003005147)
13. Brenner H. *Macrotransport processes*. Boston, MA, USA: Butterworth-Heinemann. (doi:10.1016/C2009-0-25915-0)
14. Saintillan D, Shelley MJ. 2008 Instabilities, pattern formation, and mixing in active suspensions. *Phys. Fluids* **20**, 123304. (doi:10.1063/1.3041776)
15. Subramanian G, Koch DL. 2009 Critical bacterial concentration for the onset of collective swimming. *J. Fluid Mech.* **632**, 359–400. (doi:10.1017/s002211200900706x)
16. Stenhammar J, Nardini C, Nash RW, Marenduzzo D, Morozov A. 2017 Role of correlations in the collective behavior of microswimmer suspensions. *Phys. Rev. Lett.* **119**, 028005. (doi:10.1103/physrevlett.119.028005)
17. Škultéty V, Nardini C, Stenhammar J, Marenduzzo D, Morozov A. 2020 Swimming suppresses correlations in dilute suspensions of pusher microorganisms. *Phys. Rev. X* **10**, 031059. (doi:10.1103/physrevx.10.031059)

18. Baskaran A, Cristina Marchetti M. 2010 Nonequilibrium statistical mechanics of self-propelled hard rods. *J. Stat. Mech.* **2010**, 04019. (doi:10.1088/1742-5468/2010/04/P04019)
19. Bettolo Marconi UM, Caprini L, Puglisi A. 2021 Hydrodynamics of simple active liquids: the emergence of velocity correlations. *New J. Phys*. **23**, 103024. (doi:10.1088/1367-2630/ac2b54)
20. Toner J, Tu Y. 1998 Flocks, herds, and schools: a quantitative theory of flocking. *Phys. Rev. E* **58**, E58. (doi:10.1103/physreve.58.4828)
21. Aditi Simha R, Ramaswamy S. 2002 Hydrodynamic fluctuations and instabilities in ordered suspensions of self-propelled particles. *Phys. Rev. Lett*. **89**, 058101. (doi:10.1103/physrevlett.89.058101)
22. Wensink HH, Dunkel J, Heidenreich S, Drescher K, Goldstein RE, Löwen H, Yeomans JM. 2012 Meso-scale turbulence in living fluids. *Proc. Natl Acad. Sci. USA* **109**, 14308–14313. (doi:10.1073/pnas.1202032109)
23. Dunkel J, Heidenreich S, Drescher K, Wensink HH, Bär M, Goldstein RE. 2013 Fluid dynamics of bacterial turbulence. *Phys. Rev. Lett*. **110**, 228102. (doi:10.1103/physrevlett.110.228102)
24. Doostmohammadi A, Ignés-Mullol J, Yeomans JM, Sagués F. 2018 Active nematics. *Nat. Commun*. **9**, 3246. (doi:10.1038/s41467-018-05666-8)
25. Marchetti MC, Joanny JF, Ramaswamy S, Liverpool TB, Prost J, Rao M, Simha RA. 2013 Hydrodynamics of soft active matter. *Rev. Mod. Phys*. **85**, 1143–1189. (doi:10.1103/revmodphys.85.1143)
26. Baskaran A, Marchetti MC. 2008 Hydrodynamics of self-propelled hard rods. *Phys. Rev. E* **77**, 011920. (doi:10.1103/physreve.77.011920)
27. Lauga E. 2020 *The fluid dynamics of cell motility*. Cambridge, UK: Cambridge University Press. (doi:10.1017/9781316796047)
28. Drescher K, Goldstein RE, Tuval I. 2010 Fidelity of adaptive phototaxis. *Proc. Natl Acad. Sci. USA* **107**, 11171–11176. (doi:10.1073/pnas.1000901107)
29. Drescher K, Dunkel J, Cisneros LH, Ganguly S, Goldstein RE. 2011 Fluid dynamics and noise in bacterial cell–cell and cell–surface scattering. *Proc. Natl Acad. Sci. USA* **108**, 10940–10945. (doi:10.1073/pnas.1019079108)
30. Bretherton FP. 1962 The motion of rigid particles in a shear flow at low Reynolds number. *J. Fluid Mech*. **14**, 284–304. (doi:10.1017/S002211206200124X)
31. O'Malley S, Bees MA. 2012 The orientation of swimming biflagellates in shear flows. *Bull. Math. Biol*. **74**, 232–255. (doi:10.1007/s11538-011-9673-1)
32. Ishimoto K. 2023 Jeffery's orbits and microswimmers in flows: a theoretical review. *J. Phys. Soc. Jpn*. **92**, 062001. (doi:10.7566/jpsj.92.062001)
33. Hinch EJ. 1977 An averaged-equation approach to particle interactions in a fluid suspension. *J. Fluid Mech*. **83**, 695–720. (doi:10.1017/S0022112077001414)
34. Bees MA. 2020 Advances in bioconvection. *Annu. Rev. Fluid Mech*. **52**, 449–476. (doi:10.1146/annurev-fluid-010518-040558)
35. Bruna M, Burger M, Esposito A, Schulz SM. 2022 Phase separation in systems of interacting active Brownian particles. *SIAM J. Appl. Math*. **82**, 1635–1660. (doi:10.1137/21m1452524)
36. Vrugt M te, Bickmann J, Wittkowski R. 2023 How to derive a predictive field theory for active Brownian particles: a step-by-step tutorial. *J. Phys*. **35**, 313001. (doi:10.1088/1361-648x/acc440)
37. Bees MA, Hill NA, Pedley TJ. 1998 Analytical approximations for the orientation distribution of small dipolar particles in steady shear flows. *J. Math. Biol*. **36**, 269–298. (doi:10.1007/s002850050101)
38. Kim S, Karrila SJ. 1991 *Microhydrodynamics: principles and selected applications*. Boston, MA, USA: Butterworth-Heinemann.
39. Pahlavan AA, Saintillan D. 2011 Instability regimes in flowing suspensions of swimming micro-organisms. *Phys. Fluids* **23**, 011901. (doi:10.1063/1.3529411)
40. Ezhilan B, Shelley MJ, Saintillan D. 2013 Instabilities and nonlinear dynamics of concentrated active suspensions. *Phys. Fluids* **25**, 070607. (doi:10.1063/1.4812822)
41. Saintillan D, Darve E, Shaqfeh ESG. 2005 A smooth particle-mesh Ewald algorithm for Stokes suspension simulations: the sedimentation of fibers. *Phys. Fluids* **17**, 033301. (doi:10.1063/1.1862262)
42. Doi M. 1981 Molecular dynamics and rheological properties of concentrated solutions of rodlike polymers in isotropic and liquid crystalline phases. *J. Polym. Sci*. **19**, 229–243. (doi:10.1002/pol.1981.180190205)

43. Baskaran A, Marchetti MC. 2009 Statistical mechanics and hydrodynamics of bacterial suspensions. *Proc. Natl Acad. Sci. USA* **106**, 15567–15572. (doi:10.1073/pnas.0906586106)
44. Weady S, Shelley MJ, Stein DB. 2022 A fast Chebyshev method for the Bingham closure with application to active nematic suspensions. *J. Comput. Phys*. **457**, 110937. (doi:10.1016/j.jcp.2021.110937)
45. Hinch EJ, Leal LG. 1976 Constitutive equations in suspension mechanics. Part 2. Approximate forms for a suspension of rigid particles affected by Brownian rotations. *J. Fluid Mech.* **76**, 187–208. (doi:10.1017/S0022112076003200)
46. Saintillan D, Shelley MJ. 2013 Active suspensions and their nonlinear models. *Comptes Rendus Phys*. **14**, 497–517. (doi:10.1016/j.crhy.2013.04.001)
47. Bingham C. 1974 An Antipodally Symmetric Distribution on the Sphere. *Ann. Statist.* **2**, 1201–1225. (doi:10.1214/aos/1176342874)
48. Bearon RN, Hazel AL. 2015 The trapping in high-shear regions of slender bacteria undergoing chemotaxis in a channel. *J. Fluid Mech.* **771**, R3. (doi:10.1017/jfm.2015.198)
49. Bearon RN, Hazel AL, Thorn GJ. 2011 The spatial distribution of gyrotactic swimming micro-organisms in laminar flow fields. *J. Fluid Mech.* **680**, 602–635. (doi:10.1017/jfm.2011.198)
50. Fung L, Bearon RN, Hwang Y. 2022 A local approximation model for macroscale transport of biased active Brownian particles in a flowing suspension. *J. Fluid Mech.* **935**, A24. (doi:10.1017/jfm.2022.10)
51. Rusconi R, Guasto JS, Stocker R. 2014 Bacterial transport suppressed by fluid shear. *Nat. Phys*. **10**, 212–217. (doi:10.1038/nphys2883)
52. Fung L. 2023 Analogy between streamers in sinking spheroids, gyrotactic plumes and chemotactic collapse. *J. Fluid Mech.* **961**, A12. (doi:10.1017/jfm.2023.242)
53. Childress S, Percus JK. 1981 Nonlinear aspects of chemotaxis. *Math. Biosci*. **56**, 217–237. (doi:10.1016/0025-5564(81)90055-9)
54. Masoud H, Shelley MJ. 2014 Collective surfing of chemically active particles. *Phys. Rev. Lett*. **112**, 128304. (doi:10.1103/physrevlett.112.128304)
55. Jeffrey DJ, Onishi Y. 1984 Calculation of the resistance and mobility functions for two unequal rigid spheres in low-Reynolds-number flow. *J. Fluid Mech.* **139**, 261–290. (doi:10.1017/S0022112084000355)
56. Papavassiliou D, Alexander GP. 2017 Exact solutions for hydrodynamic interactions of two squirming spheres. *J. Fluid Mech*. **813**, 618–646. (doi:10.1017/jfm.2016.837)
57. Li Sing How M, Koch DL, Collins LR. 2021 Non-continuum tangential lubrication gas flow between two spheres. *J. Fluid Mech.* **920**, A2. (doi:10.1017/jfm.2021.308)
58. Ball RC, Melrose JR. 1995 Lubrication breakdown in hydrodynamic simulations of concentrated colloids. *Adv. Colloid Interface Sci*. **59**, 19–30. (doi:10.1016/0001-8686(95)80003-l)
59. Brady JF, Morris JF. 1997 Microstructure of strongly sheared suspensions and its impact on rheology and diffusion. *J. Fluid Mech*. **348**, 103–139. (doi:10.1017/s0022112097006320)
60. te Vrugt M, Löwen H, Wittkowski R. 2020 Classical dynamical density functional theory: from fundamentals to applications. *Adv. Phys*. **69**, 121–247. (doi:10.1080/00018732.2020.1854965)
61. Goddard BD, Nold A, Savva N, Pavliotis GA, Kalliadasis S. 2012 General dynamical density functional theory for classical fluids. *Phys. Rev. Lett*. **109**, 120603. (doi:10.1103/physrevlett.109.120603)
62. Wensink HH, Löwen H. 2008 Aggregation of self-propelled colloidal rods near confining walls. *Phys. Rev. E* **78**, 031409. (doi:10.1103/physreve.78.031409)
63. Menzel AM, Saha A, Hoell C, Löwen H. 2016 Dynamical density functional theory for microswimmers. *J. Chem. Phys*. **144**, 024115. (doi:10.1063/1.4939630)
64. Bruna M, Chapman SJ. 2012 Excluded-volume effects in the diffusion of hard spheres. *Phys. Rev. E* **85**, 011103. (doi:10.1103/physreve.85.011103)
65. Lauga E, DiLuzio WR, Whitesides GM, Stone HA. 2006 Swimming in circles: motion of bacteria near solid boundaries. *Biophys. J*. **90**, 400–412. (doi:10.1529/biophysj.105.069401)
66. Berke AP, Turner L, Berg HC, Lauga E. 2008 Hydrodynamic attraction of swimming microorganisms by surfaces. *Phys. Rev. Lett*. **101**, 1–4. (doi:10.1103/physrevlett.101.038102)

67. Hill J, Kalkanci O, McMurry JL, Koser H. 2007 Hydrodynamic surface interactions enable *Escherichia coli* to seek efficient routes to swim upstream. *Phys. Rev. Lett*. **98**, 068101. (doi:10.1103/PhysRevLett.98.068101)
68. Rusconi R, Stocker R. 2015 Microbes in flow. *Curr. Opin. Microbiol*. **25**, 1–8. (doi:10.1016/j.mib.2015.03.003)
69. Sauer K, Stoodley P, Goeres DM, Hall-Stoodley L, Burmølle M, Stewart PS, Bjarnsholt T. 2022 The biofilm life cycle: expanding the conceptual model of biofilm formation. *Nat. Rev. Microbiol*. **20**, 608–620. (doi:10.1038/s41579-022-00767-0)
70. Maleki A, Ghodrat M, Pagonabarraga I. 2024 Activity-induced asymmetric dispersion in confined channels with constriction. *Phys. Rev. Fluids* **9**, 013103. (doi:10.1103/physrevfluids.9.013103)
71. Ostapenko T, Schwarzendahl FJ, Böddeker TJ, Kreis CT, Cammann J, Mazza MG, Bäumchen O. 2018 Curvature-guided motility of microalgae in geometric confinement. *Phys. Rev. Lett*. **120**, 068002. (doi:10.1103/physrevlett.120.068002)
72. Chen H, Thiffeault JL. 2021 Shape matters: a Brownian microswimmer in a channel. *J. Fluid Mech*. **916**, A15. (doi:10.1017/jfm.2021.144)
73. Zeng L, Jiang W, Pedley TJ. 2022 Sharp turns and gyrotaxis modulate surface accumulation of microorganisms. *Proc. Natl Acad. Sci. USA* **119**, e2206738119. (doi:10.1073/pnas.2206738119)
74. Aranson IS. 2022 Bacterial active matter. *Rep. Prog. Phys*. **85**, 076601. (doi:10.1088/1361-6633/ac723d)
75. Lauga E. 2016 Bacterial hydrodynamics. *Annu. Rev. Fluid Mech*. **48**, 105–130. (doi:10.1146/annurev-fluid-122414-034606)
76. Elgeti J, Winkler RG, Gompper G. 2015 Physics of microswimmers—single particle motion and collective behavior: a review. *Rep. Prog. Phys*. **78**, 056601. (doi:10.1088/0034-4885/78/5/056601)
77. Li G, Tang JX. 2009 Accumulation of microswimmers near a surface mediated by collision and rotational Brownian motion. *Phys. Rev. Lett*. **103**, 078101. (doi:10.1103/physrevlett.103.078101)
78. Spagnolie SE, Lauga E. 2012 Hydrodynamics of self-propulsion near a boundary: predictions and accuracy of far-field approximations. *J. Fluid Mech*. **700**, 105–147. (doi:10.1017/jfm.2012.101)
79. Costanzo A, Di Leonardo R, Ruocco G, Angelani L. 2012 Transport of self-propelling bacteria in micro-channel flow. *J. Phys*. **24**, 065101. (doi:10.1088/0953-8984/24/6/065101)
80. Elgeti J, Gompper G. 2013 Wall accumulation of self-propelled spheres. *EPL* **101**, 48003. (doi:10.1209/0295-5075/101/48003)
81. Ezhilan B, Saintillan D. 2015 Transport of a dilute active suspension in pressure-driven channel flow. *J. Fluid Mech*. **777**, 482–522. (doi:10.1017/jfm.2015.372)
82. Kantsler V, Dunkel J, Polin M, Goldstein RE. 2013 Ciliary contact interactions dominate surface scattering of swimming eukaryotes. *Proc. Natl Acad. Sci. USA* **110**, 1187–1192. (doi:10.1073/pnas.1210548110)
83. Molaei M, Barry M, Stocker R, Sheng J. 2014 Failed escape: solid surfaces prevent tumbling of *Escherichia coli*. *Phys. Rev. Lett*. **113**, 068103. (doi:10.1103/physrevlett.113.068103)
84. Contino M, Lushi E, Tuval I, Kantsler V, Polin M. 2015 Microalgae scatter off solid surfaces by hydrodynamic and contact forces. *Phys. Rev. Lett*. **115**, 258102. (doi:10.1103/physrevlett.115.258102)
85. Bianchi S, Saglimbeni F, Di Leonardo R. 2017 Holographic imaging reveals the mechanism of wall entrapment in swimming bacteria. *Phys. Rev. X* **7**, 011010. (doi:10.1103/physrevx.7.011010)
86. Walker BJ, Ishimoto K, Gaffney EA. 2023 Systematic parameterizations of minimal models of microswimming. *Phys. Rev. Fluids* **8**, 034102. (doi:10.1103/physrevfluids.8.034102)
87. Leishangthem P, Xu X. 2024 Thermodynamic effects are essential for surface entrapment of bacteria. *Phys. Rev. Lett*. **132**, 238302. (doi:10.1103/PhysRevLett.132.238302)
88. Schaar K, Zöttl A, Stark H. 2015 Detention times of microswimmers close to surfaces: influence of hydrodynamic interactions and noise. *Phys. Rev. Lett*. **115**, 038101. (doi:10.1103/physrevlett.115.038101)
89. Hernandez-Ortiz JP, Underhill PT, Graham MD. 2009 Dynamics of confined suspensions of swimming particles. *J. Phys*. **21**, 204107. (doi:10.1088/0953-8984/21/20/204107)

90. Sepúlveda N, Soto R. 2018 Universality of active wetting transitions. *Phys. Rev. E* **98**, 052141. (doi:10.1103/physreve.98.052141)
91. Poortinga AT, Bos R, Norde W, Busscher HJ. 2002 Electric double layer interactions in bacterial adhesion to surfaces. *Surf. Sci. Rep*. **47**, 1–32. (doi:10.1016/s0167-5729(02)00032-8)
92. Elgeti J, Gompper G. 2009 Self-propelled rods near surfaces. *EPL* **85**, 38002. (doi:10.1209/0295-5075/85/38002)
93. Schuss Z. 2013 *Brownian dynamics at boundaries and interfaces*. New York, NY, USA: Springer New York.(Applied mathematical sciences). (doi:10.1007/978-1-4614-7687-0)
94. Jiang W, Chen G. 2019 Dispersion of active particles in confined unidirectional flows. *J. Fluid Mech*. **877**, 1–34. (doi:10.1017/jfm.2019.562)
95. Elgeti J, Gompper G. 2016 Microswimmers near surfaces. *Eur. Phys. J. Spec. Top*. **225**, 2333–2352. (doi:10.1140/epjst/e2016-60070-6)
96. Rothschild. 1963 Non-random distribution of bull spermatozoa in a drop of sperm suspension. *Nature* **200**, 1221–1222. (doi:10.1038/200381a0)
97. Maretvadakethope S, Hazel AL, Vasiev B, Bearon RN. 2023 The interplay between bulk flow and boundary conditions on the distribution of microswimmers in channel flow. *J. Fluid Mech.* **976**, A13. (doi:10.1017/jfm.2023.897)
98. Volpe G, Gigan S, Volpe G. 2014 Simulation of the active Brownian motion of a microswimmer. *Am. J. Phys*. **82**, 659–664. (doi:10.1119/1.4870398)
99. Jiang W, Chen G. 2020 Dispersion of gyrotactic micro-organisms in pipe flows. *J. Fluid Mech.* **889**, A18. (doi:10.1017/jfm.2020.91)
100. Wang B, Jiang W, Chen G, Tao L. 2022 Transient dispersion in a channel with crossflow and wall adsorption. *Phys. Rev. Fluids* **7**, 074501. (doi:10.1103/physrevfluids.7.074501)
101. Zeriouh O, Reinoso-Moreno JV, López-Rosales L, Cerón-García M del C, Sánchez-Mirón A, García-Camacho F, Molina-Grima E. 2017 Biofouling in photobioreactors for marine microalgae. *Crit. Rev. Biotechnol*. **37**, 1006–1023. (doi:10.1080/07388551.2017.1299681)
102. Sankarasubramanian R. 1973 Unsteady convective diffusion with interphase mass transfer. *Proc. R. Soc. Lond. A* **333**, 115–132. (doi:10.1098/rspa.1973.0051)
103. Shapiro M, Brenner H. 1987 Chemically reactive generalized Taylor dispersion phenomena. *AIChE J.* **33**, 1155–1167. (doi:10.1002/aic.690330710)
104. Lin TY, Shaqfeh ESG. 2019 Taylor dispersion in the presence of cross flow and interfacial mass transfer. *Phys. Rev. Fluids* **4**, 034501. (doi:10.1103/physrevfluids.4.034501)
105. Ishikawa T, Simmonds MP, Pedley TJ. 2006 Hydrodynamic interaction of two swimming model micro-organisms. *J. Fluid Mech*. **568**, 119–160. (doi:10.1017/S0022112006002631)
106. Schoeller SF, Keaveny EE. 2018 From flagellar undulations to collective motion: predicting the dynamics of sperm suspensions. *J. R. Soc. Interface* **15**, 20170834. (doi:10.1098/rsif.2017.0834)